ACS OMEGA

Open Access

This article is licensed under CC-BY-NC-ND 4.0

http://pubs.acs.org/journal/acsodf

Article

A Site-Specific Cross-Linker for Visible-Light Control of Proteins

Zhuangyu Zhao, Nathan A. Rudman, and Ivan J. Dmochowski*

Cite This: *ACS Omega* 2024, 9, 29331−29338

Read Online

ACCESS | Metrics & More | Article Recommendations | Supporting Information

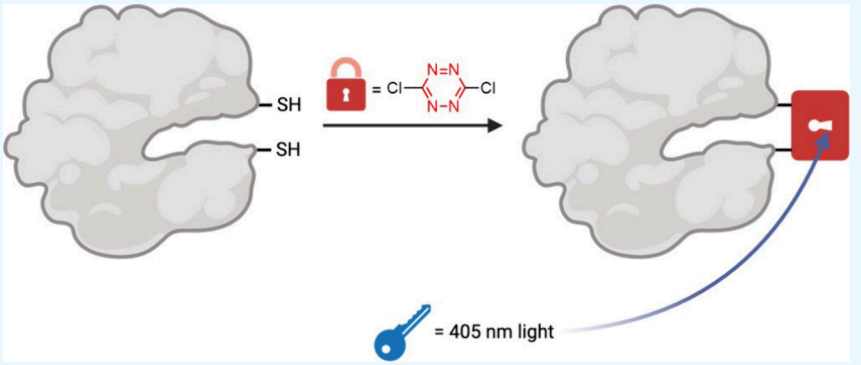

ABSTRACT: There is a need for photochemical tools that allow precise control of protein structure and function with visible light. We focus here on the *s*-tetrazine moiety, which can be installed at a specific protein site via the reaction between dichlorotetrazine and two adjacent sulfhydryl groups. Tetrazine's compact size enables structural mimicry of native amino acid linkages, such as an intramolecular salt bridge or disulfide bond. In this study, we investigated tetrazine installation in three different proteins, where it was confirmed that the cross-linking reaction is highly efficient in aqueous conditions and site-specific when two cysteines are located proximally: the S−S distance was 4−10 Å. As shown in maltose binding protein, the tetrazine cross-linker can replace an interdomain salt bridge crucial for xenon binding and serve as a visible-light photoswitch to modulate ^{129}Xe NMR contrast. This work highlights the ease of aqueous tetrazine bioconjugation and its applications for protein photoregulation.

INTRODUCTION

Optical manipulation of proteins can reveal functional significance in normal and diseased cells.[1] Orthogonal to many other stimuli, light conveniently provides wavelength-selective regulation of photoactive molecules.[2−5] Many light-responsive methods have been developed to manipulate protein binding affinity,[6,7] protein folding,[8−12] bioactivity,[13−15] and signaling.[16−18] Optical control of proteins can be achieved by (a) fusion to naturally occurring photosensitive proteins, such as light-oxygen-voltage (LOV) domains,[19−21] or (b) introduction of photoresponsive small molecules via genetic encoding or chemical modification.[13,15,22−24] While it is convenient to borrow photoresponsive proteins from nature, challenges remain such as choosing suitable insertion sites and tuning chromophore properties. Notably, photoactive small molecules offer site-specific modulation with increased stability and enable more adaptable and predictable functionalization of proteins.

Photoresponsive chemical modifications can be categorized as photoswitchable[25−27] or photocleavable[28−31] compounds. Photoswitchable compounds are predominantly based on azobenzene, which can isomerize between *cis* and *trans* conformations upon light irradiation, causing a substantial, ∼7 Å change in length. This switch in molecular geometry can reversibly obstruct a protein functional site or induce protein conformational changes to alter structure and function.[14,16] Unlike photoswitches, photocleavable moieties undergo bond cleavage when exposed to light; thus, they are often tethered as protecting groups on a protein functional site.[32−35] Among the available photocleavable moieties, *o*-nitrobenzyl compounds, coumarin derivatives, and other aromatic ketones, esters and ethers are the most reliable and widely used structures.[28,30,31] However, the photolysis of these photolabile compounds usually requires UV wavelengths. In addition, bifunctional cross-linkers containing *o*-nitrobenzyl or other photocleavable moieties are often difficult to insert within proteins due to their large size.[29] To expand the photochemical toolkit for biochemistry, bifunctional phototriggers that are responsive to visible light are needed for manipulating protein structures and dynamics.

Received: January 30, 2024
Revised: March 5, 2024
Accepted: March 13, 2024
Published: June 28, 2024

© 2024 The Authors. Published by American Chemical Society

The versatile *s*-tetrazine molecule has been widely explored for the creation of functional molecules and materials.[36,37] It was first introduced by Smith and Hochstrasser as an ultrafast photoreleasable chromophore to probe peptide folding and dynamics,[12,38−41] in addition to its use as a bioorthogonal conjugation handle via the inverse Diels−Alder reaction.[42,43] Synthetic protocols were developed to allow rapid incorporation of the compact (∼3 Å) *s*-tetrazine linker within peptides containing two proximal cysteines. The resulting *S*,*S*-tetrazine moiety can be optimally photolyzed using near-UV light (355 nm) or visible blue light (410 nm) to restore the linear peptide conformation, followed by regeneration of the native peptide using cysteine.[40] Two notable limitations were a decrease in conjugation efficiency with increasing distance between the cysteines and the requirement of solid-phase peptide synthesis or an organic-phase reaction. Attempts to incorporate *s*-tetrazine into the active site of a thioredoxin protein in aqueous solution did not produce the desired photolytic results.[40] Notably, a recent study developed photocleavable hydrogels based on tetrazine-thiol cross-linking in phosphate-buffered saline and found that green light (532 nm) can efficiently degrade the hydrogels *in vivo*, enabling precise photocontrol of drug release.[44]

In the present work, we investigate the incorporation of the tetrazine phototrigger under aqueous conditions within three different proteins: yeast copper chaperone (Atx1), ribose binding protein (RBP), and maltose binding protein (MBP). Atx1 is a small 8 kDa protein with a well-characterized, solvent-accessible CXXC motif. We tested the feasibility of inserting tetrazine between these proximal native cysteines under aqueous conditions. Then, the tetrazine cross-linker was used to replace and mimic intramolecular interactions in RBP and MBP, which belong to the family of periplasmic binding proteins and undergo large domain movement upon ligand binding. Wild-type RBP and MBP have no Cys residues, and suitable tetrazine insertion sites were identified via molecular dynamics (MD) simulations. Notably, MBP is a useful genetically encoded contrast agent for ^{129}Xe NMR spectroscopy,[45] due to regulation of Xe exchange by a switchable salt bridge.[46] Here, we show optical control of the magnetic resonance (MR) contrast in MBP by replacing this salt bridge with a tetrazine moiety.

RESULTS AND DISCUSSION

Incorporation of the Tetrazine Cross-Linker into Atx1 Protein under Aqueous Conditions. The investigation of tetrazine reaction with Atx1 was designed to test the cross-linking efficiency in aqueous solution. This yeast homologue of the human Atox1 metallochaperone has two native Cys residues (C15 and C18) in its copper binding site. The close distance between C15 and C18 suggested that this site should be compatible with insertion of a tetrazine cross-linker. We prepared freshly reduced Atx1 protein in acetate buffer and incubated with equimolar dichlorotetrazine at room temperature (Scheme 1). Considering the reactivity of the highly electrophilic dichlorotetrazine moiety toward non-Cys residues in the protein and solvent molecules in aqueous buffer, and also the strong potential for protein dimerization due to intermolecular cross-linking, we analyzed the reaction mixture by 5,5′-dithio-bis-[2-nitrobenzoic acid] (DTNB) assay and size exclusion chromatography. Under optimized conditions, near-stoichiometric cross-linking was observed with a remaining active thiol content measured by the DTNB assay of only 3% of total Cys residues. The yield of the cross-linked product Atx1-Tz was estimated to be ∼97% by size exclusion chromatography where Atx1-Tz eluted at a retention volume (V_R = 88.24 mL; Figure S1a) similar to monomeric native Atx1 (V_R = 89.07 mL; Figure S1b), as monitored by 280 nm (protein and tetrazine) and 410 nm (tetrazine) absorptions. SDS-PAGE analysis of the major product revealed a molecular weight of approximately 8 kDa (Figure S2), confirming the absence of intermolecular cross-linking.

Scheme 1. Tetrazine Insertion between Di-Cysteine Side Chains of the CXXC Motif (Yellow) in Atx1

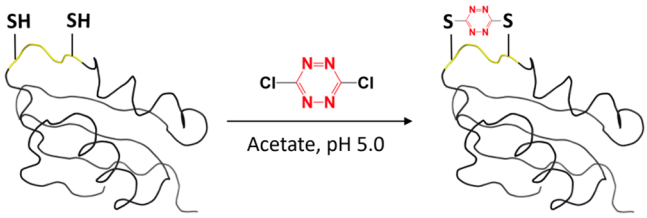

The identity of purified Atx1-Tz was confirmed by the characteristic tetrazine absorption bands at 419 and 514 nm (Figure 1, black spectrum). Tetrazine incorporation was confirmed by MALDI-TOF mass spectrometry (Figure S3a), and this caused minimal perturbation to the protein secondary structure at room temperature according to circular dichroism (CD) spectroscopy (Figure S3b). The Atx1-Tz sample also lost its copper binding affinity (Figure S4), consistent with complete cross-linking of the Cys side chains. These results demonstrate that the tetrazine cross-linker can be readily installed into protein at a specific site with high efficiency in aqueous solution.

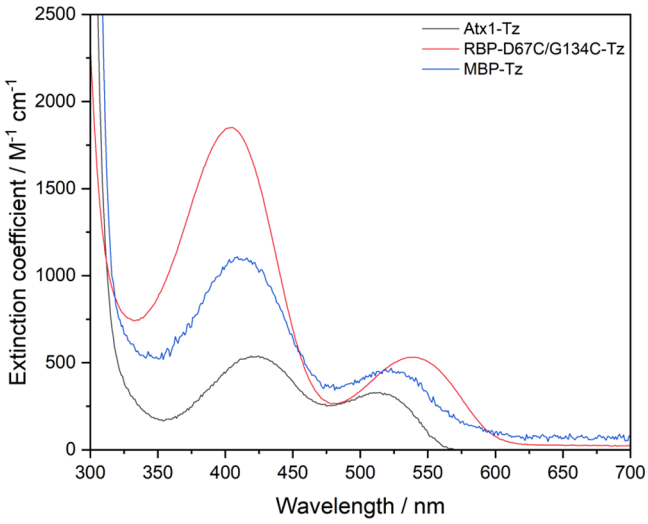

Figure 1. UV−vis absorption spectra of Atx1-Tz (black), RBP-D67C/G134C-Tz (red), and MBP-Tz (blue).

Replacement of Intramolecular Salt Bridges in RBP. Having established a method for incorporation of tetrazine into a protein with a conserved CXXC motif under aqueous conditions, we set out to introduce the tetrazine cross-linker into proteins that natively lack cysteine. By engineering site-specific cysteine mutations, it is possible to install tetrazine at an arbitrary site and achieve control over the protein structure and function.

https://doi.org/10.1021/acsomega.4c00968
ACS Omega 2024, 9, 29331−29338

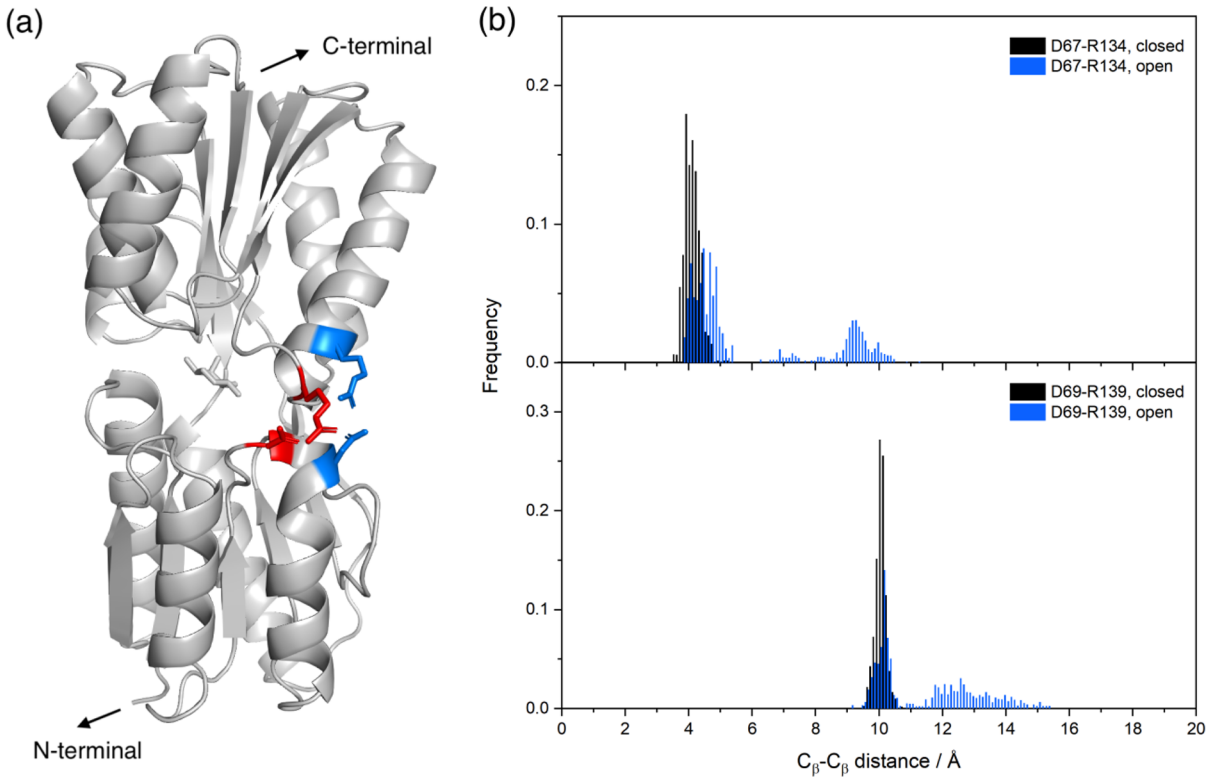

Figure 2. Identification of interdomain salt bridges as potential sites for tetrazine installation by MD simulations. (a) Structural illustration of two interdomain salt bridges in RBP-G134R: D67-R134 (red sticks) and D69-R139 (blue sticks). (b) C_β−C_β distances calculated for D67-R134 (top) and D69-R139 (bottom) in the closed state (black) and open state (blue) of RBP.

In native RBP, binding to the ribose ligand induces a significant interdomain motion of at least 43° along the interdomain rotational axis.[47] Using computational methods, we identified salt bridge interactions that form concomitantly with RBP's domain closure and can be substituted with the covalent tetrazine cross-linker to lock in the "closed" protein conformation. MD simulations of the RBP G134R mutant[43] in the absence and presence of bound ribose identified two interdomain salt bridges, D67-R134 and D69-R139, within the ligand binding cleft (Figure 2a). Examination of the C_β−C_β distance of each pair suggested that D67-R134 and D69-R139 formed closer interactions upon domain closure (Figure 2b). The average C_β−C_β distance of the D67-R134 salt bridge was ∼4 Å in the closed conformation, whereas the C_β−C_β distance of D69-R139 was ∼10 Å.

To investigate the efficiency of tetrazine incorporation at different sites, we replaced interdomain salt bridge D67-R134 or D69-R139 of RBP with a pair of cysteine residues as reaction handles. Given that the distance between C67 and C134 side chains is shorter than the C69−C139 pair, it was predicted that the D67C/G134C site should have a higher cross-linking efficiency. Using similar bioconjugation procedures to those that were optimized for tetrazine incorporation into Atx1, the DTNB assay revealed that the remaining unreacted thiol content was ∼13% in RBP-D67C/G134C and ∼43% in RBP-D69C/R139C. Hence, to remove protein containing unreacted thiols, we used a scavenger polymer, PEG-MAL, which has eight polyethylene maleimide arms to react with active thiols and forms large protein oligomers that can be easily separated from monomeric protein. After incubation with the PEG-MAL polymer and separation using size exclusion chromatography, pure RBP-D67C/G134C-Tz was obtained in ∼50% yield (Figure S5a), whereas RBP-D69C/R139C-Tz had a much lower yield of ∼5% (Figure S5b), in agreement with prediction. The low yields of both RBP mutants also suggested the presence of side reactions, such as intermolecular cross-linking and potential hydrolysis. RBP-D69C/R139C-Tz was not further characterized due to its low yield. Identity of RBP-D67C/G134C-Tz was confirmed by MALDI-TOF mass spectrometry (Figure S6), SDS-PAGE (Figure S7), and absence of active thiols in the DTNB assay. The purified RBP-Tz showed an n−π^* transition at 540 nm and a π−π^* transition at 405 nm (Figure 1, red spectrum). The bathochromic shift of the n−π^* transition and the hypsochromic shift of the π−π^* transition in comparison to Atx1-Tz were consistent with a less solvent-accessible cross-linking site in RBP-Tz. These results confirmed that the tetrazine cross-linker can be used to replace buried salt bridge interactions in proteins, and the cross-linking efficiency depends on the distance between the bridging sulfur atoms, over a range of 4 to 10 Å.

Optical Control of MR Contrast in MBP. To demonstrate a useful application of tetrazine cross-linking and photocleavage in protein, we introduced the cross-linker into MBP, which belongs to the family of periplasmic binding proteins, similar to RBP, and also serves as a ^{129}Xe NMR contrast agent. Our laboratory has shown previously that MBP can exhibit a strong hyperpolarized ^{129}Xe chemical exchange saturation transfer (hyper-CEST) response upon maltose binding, and its K15-E111 salt bridge regulates the xenon−protein interaction that is responsible for the ^{129}Xe NMR signal.[45,46] Therefore, we chose this site for tetrazine cross-linking to enable photocontrol over MR contrast. Similar to RBP, wild-type MBP has no cysteine; thus, K15 and E111 were

https://doi.org/10.1021/acsomega.4c00968
ACS Omega 2024, 9, 29331−29338

mutated to cysteines (K15C/E111C) as reactive sites for tetrazine cross-linking. Following the aforementioned aqueous cross-linking procedures, the desired bis-conjugated product (MBP-Tz) was purified in ∼40% yield, and its identity was verified by MALDI-TOF mass spectrometry (Figure S8). The DTNB assay showed the absence of active cysteine, and enzymatic digestion confirmed the intraprotein cross-linking sites (Figure S9). The secondary structure of the cross-linked protein, measured by CD spectroscopy, resembled the native, non-cross-linked protein (Figure S10), suggesting that protein structural integrity was maintained. Moreover, the tetrazine moiety gave rise to an increase of the molar extinction coefficient at 280 nm by 8030 M^{-1} cm^{-1}, determined by the Bradford assay. The characteristic $\pi-\pi^*$ and $n-\pi^*$ absorption bands of *S*,*S*-tetrazine were observed at 409 and 523 nm (Figure 1, blue), with molar extinction coefficients of 1100 and 470 M^{-1} cm^{-1}, respectively, in good agreement with previous tetrazine-peptide studies.[40]

To evaluate the effect of the tetrazine cross-linker on the xenon−MBP interaction, the hyper-CEST z-spectra were obtained using 80 μM reduced native MBP-K15C/E111C (as a negative control) and the purified cross-linked product MBP-Tz (Figure 3). Notably, tetrazine cross-linking produced

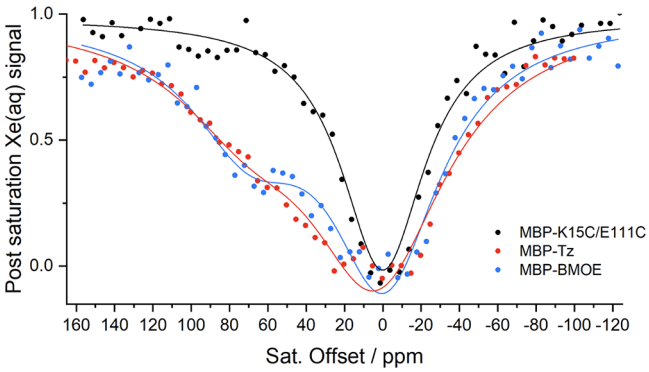

Figure 3. Hyper-CEST z-spectra of 80 μM non-cross-linked MBP-K15C/E111C (black), MBP-Tz (red), and MBP-BMOE (blue) in PBS (pH 7.4) at 298 K.

a broad ^{129}Xe NMR signal centered at +60 ppm, referenced to free ^{129}Xe dissolved in PBS. The saturation frequency of ^{129}Xe@MBP-Tz shifted differently compared to maltose-bound wild-type MBP (+90 ppm),[45] which results from a slightly perturbed environment of the xenon cavity.[48] Importantly, xenon was sufficiently confined by the tetrazine-cross-linked protein to give a measurable hyper-CEST signal in the absence of maltose. Therefore, MBP-Tz-mediated ^{129}Xe saturation transfer could be measured as hyper-CEST saturation contrast, representing the normalized difference between on-resonance and off-resonance signals. For the tetrazine-cross-linked MBP sample, a saturation contrast of 0.72 ± 0.04 at 10 μM concentration was observed by time-dependent saturation transfer experiments using ±60 ppm saturation pulses (Figure 4 and Figure S11). This highlights the ability to detect MBP protein samples at low micromolar and even lower concentrations using ultrasensitive hyperpolarized ^{129}Xe NMR techniques. Notably, mammalian cells lack maltose, which prevents wild-type MBP from being useful as an *in vivo* ^{129}Xe MRI contrast agent. This study highlights that MBP-Tz circumvents the requirement for maltose to generate the ^{129}Xe

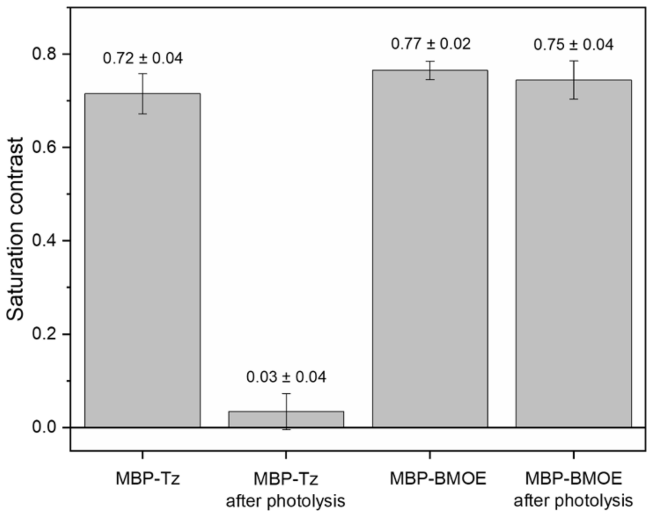

Figure 4. Hyper-CEST saturation contrast of 10 μM MBP-Tz and MBP-BMOE before and after photolysis.

NMR signal and provides a strategy for generating protein contrast agents for future *in vivo* imaging studies.

After confirming the ability of tetrazine cross-linking to replicate the xenon−MBP interaction that has been established for maltose-bound MBP, we tested the photolysis of MBP-Tz with 405 nm blue light (Figure S12). The photolytic reaction followed the model of a first-order reaction with a quantum yield of ∼10^{-4}, as monitored by UV−vis absorption at 280, 320, and 410 nm (Figure S13). Complete photolysis led to disappearance of the two visible absorption bands of *S*,*S*-tetrazine at 410 and 532 nm and emergence of a new product absorption peak at 320 nm. The molar extinction coefficient of the postphotolytic protein at 280 nm (66,780 M^{-1} cm^{-1}) recovered to a value similar to that of native non-cross-linked protein (67,840 M^{-1} cm^{-1}), confirming removal of the tetrazine species. Consistent with complete photocleavage, xenon was no longer confined in the protein: Saturation contrast employing ^{129}Xe NMR essentially vanished (0.03 ± 0.04) at a 10 μM concentration (Figure 4 and Figure S11b). Although MBP-Tz did not form significant oligomerization or aggregation products after photolysis, as determined by SDS-PAGE and dynamic light scattering (Figures S14 and S15), a significant change in CD (∼30% loss of signal at 222 nm) was observed (Figure S16a). To assess whether the protein structure can be photochemically damaged by 405 nm irradiation, we subjected bismaleimidoethane-cross-linked protein (MBP-BMOE) to the same photolysis conditions. BMOE is a short (∼8 Å) bifunctional cross-linker with no photoactivity and can be incorporated between Cys-15 and Cys-111 with near-stoichiometric efficiency. MBP-BMOE produced a similar xenon−MBP interaction, as a ^{129}Xe hyper-CEST signal at +65 ppm was observed (Figure 3 and Figure S17). However, saturation contrast remained the same before (0.77 ± 0.02) and after (0.75 ± 0.04) photolysis (Figure 4 and Figure 11), and only a minimal difference in the CD signal was observed (Figure S16b). Hence, without the photoactive tetrazine moiety, 405 nm light had no effect on the ^{129}Xe signal and protein integrity. In addition, no CD signal changes upon photolysis were observed in RBP-D67C/G134C-Tz (Figure S18), which lacks a Trp residue. The heightened photolytic damage to MBP-Tz may be attributed to the photochemical reactivity of tetrazine toward tryptophan

https://doi.org/10.1021/acsomega.4c00968
ACS Omega 2024, 9, 29331−29338

residues under the required aerobic photolysis conditions.[40] However, the mass spectrometric analysis of the resulting product was elusive (Figure S8) due to possible formation of multiple photolytic products. Further investigation should address the issue of photolytic damage in order to achieve effective regeneration of the unlabeled protein.

These results demonstrate that tetrazine cross-linker can be used to mimic the switchable K15-E111 salt bridge and regulate ^{129}Xe NMR contrast via blue light irradiation.

CONCLUSIONS

In summary, the photocleavable tetrazine cross-linker was successfully installed at specific sites in three different proteins. Our results show that incorporation of tetrazine under aqueous conditions can reach near-stoichiometric efficiency in Atx1, leading to inactivation of the copper binding site. The covalent bifunctional tetrazine cross-linker can also be introduced into Cys-free proteins, such as RBP and MBP, to replace the specific interdomain salt bridges predicted computationally. Cross-linking efficiency is sensitive to the distance between bridging cysteine side chains, and it is convenient that the size of the compact tetrazine cross-linker is comparable to the distance of typical intramolecular interactions, such as disulfide linkages and salt bridges. As a result of covalent coupling of tetrazine at a proper site, MBP-Tz is ^{129}Xe NMR-active, giving strong hyper-CEST contrast at +60 ppm downfield from the water signal. The tetrazine phototrigger can be efficiently cleaved upon exposure to 405 nm blue light, enabling MBP-Tz to serve as a photoresponsive NMR contrast agent, with 96% loss of NMR contrast postphotolysis (0.72 ± 0.04 versus 0.03 ± 0.04, Figure 4). By comparison, a near-complete reduction of NMR/MRI contrast is difficult to achieve using more conventional relaxivity-based contrast agents. For example, a photoactive gadolinium-based MRI contrast agent yielded a 61% decrease in water relaxivity.[49] Finally, using the synthesis, purification, and characterization strategies developed here, the concept of tetrazine-protein cross-linker can be expanded more broadly as a versatile photochemical tool in protein manipulation.

EXPERIMENTAL PROCEDURES

MD Simulations. MD simulations were performed with NAMD software[50] using the Bridges-2 Regular Memory system at the Pittsburgh Supercomputing Center (PSC).[51,52] Initial structures were obtained by modifying the crystal structure of RBP with the G134R mutation (PDB: 1DRJ) using PyMOL. Each protein was then solvated in a TIP3P water box[53] and 150 mM NaCl was used to neutralize total charge. Each system was minimized with 1000 steps, after which the system was equilibrated at a temperature of 300 K and a pressure of 1 atm using the Langevin thermostat and barostat methods. The CHARMM36 force field was used to perform all MD simulations.[54] The Xe atom was treated with only nonbonded interactions.[55] Periodic boundary conditions were employed, and the SHAKE algorithm[56] was applied to constrain the lengths of all bonds that involve a hydrogen. Salt-bridge distances and RMSF data were calculated using VMD 1.9.3.[57]

Plasmid Preparation. The Atx1, RBP-D67C/G134C, and RBP-L19A/D67C/G134C genes were synthesized by Integrated DNA Technologies, Inc. and inserted into the pET expression vector between *Bgl*II and *Hin*dIII restriction sites. K15C and E111C mutations were introduced to the pET His6MBP TEV LIC cloning vector, a gift from Scott Gradia acquired via Addgene (#29656), using the forward and reverse primers listed in Table S1. The mutated plasmids were amplified in NEB 5α competent *Escherichia coli* cells (New England Biolabs) and purified using a miniprep kit (Qiagen). All mutated sequences were verified at the University of Pennsylvania DNA Sequencing Facility.

Protein Expression and Purification. Atx1 was expressed using the *E. coli* BL21(DE3) expression system. Protein expression was induced by 1 mM isopropyl-β-D-thiogalactoside (IPTG), and induced cells were incubated overnight at 25 °C, harvested by centrifugation, and frozen at −80 °C. The cell lysate was extracted by three freeze−thaw cycles in 20 mM MES (pH 6.0) and 1 mM TCEP. After centrifugation, clear lysate was applied to a cation exchange column (HiTrap CM Sepharose FF, Cytiva) pre-equilibrated with 20 mM MES (pH 6.0), 1 mM EDTA, and 1 mM TCEP. The Atx1 protein was eluted by an increasing gradient from 0 to 0.5 M NaCl. Fractions containing Atx1 were then collected, concentrated, and further purified by size-exclusion chromatography (HiLoad 16/600 Superdex 75 pg column, GE Life Sciences) using 20 mM MES (pH 6.0), 0.1 M NaCl, and 1 mM TCEP. Protein purity was analyzed by SDS-PAGE (Figure S2). Protein concentrations were determined from the absorbance at 280 nm using the extinction coefficient 4470 M^{-1} cm^{-1}, as calculated by PROTPRAM.[58]

MBP-K15C/E111C was expressed and purified using the same procedures for wt-MBP.[45] Briefly, the plasmid encoding the sequence of MBP-K15C/E111C was transformed into BL21(DE3) competent *E. coli* cells (New England Biolabs) and grown in three 1 L flasks of LB media supplemented with 50 μg/mL kanamycin. Protein expression was induced by adding 1 mM IPTG. The induced cells were incubated overnight at 25 °C, harvested by centrifugation, and frozen at −80 °C. The cell pellets were resuspended in 20 mM sodium phosphate (pH 7.4), lysed with hen egg white lysozyme (Alfa Aesar), and treated with benzonase nuclease (Sigma). The lysate was stirred for 30 min, and 500 mM NaCl was added before clarification by centrifugation at 13,000 rpm. The supernatant was loaded onto a Ni column (HisTrap HP, Cytiva) pre-equilibrated with 20 mM sodium phosphate (pH 7.4) and 500 mM NaCl. MBP-K15C/E111C was eluted by supplementation with 500 mM imidazole. The eluate containing MBP-K15C/E111C protein was concentrated and reduced using 2 mM TCEP. The protein was further purified by size-exclusion chromatography (HiLoad 16/600 Superdex 75 pg column, GE Life Sciences) in PBS (pH 7.4). Pure apo protein (as evidenced by SDS-PAGE; Figure S13A) was pooled and concentrated. Protein concentrations were determined from the absorbance at 280 nm using the extinction coefficient 67,840 M^{-1} cm^{-1}, as calculated by PROTPRAM.[58]

RBP-D67C/G134C and RBP-L19A/D67C/G134C expression and purification followed similar procedures to MBP-K15C/E111C. Urea was used to remove endogenous ribose on-column during His-tag purification. Protein purity was confirmed by SDS-PAGE (Figure S7). Protein concentrations were determined from the absorbance at 280 nm using the extinction coefficient 5960 M^{-1} cm^{-1}, as calculated by PROTPRAM.[58]

Conjugation of Tetrazine and BMOE. Stock solutions of 3,6-dichloro-1,2,4,5-tetrazine (ChemScene) and BMOE (bis-

https://doi.org/10.1021/acsomega.4c00968
ACS Omega 2024, 9, 29331−29338

maleimidoethane, Thermo Scientific) were prepared in DMSO. Freshly purified protein was prepared at 50−100 μM in acetate (pH 5.0) buffer and PBS (pH 7.4), followed by the addition of equimolar dichlorotetrazine and BMOE, respectively. The final concentration of DMSO was no more than 2%. The tetrazine reaction mixture was buffer exchanged to PBS (pH 7.4) and treated with the 8-arm PEG-maleimide (tripentaerythritol core) polymer (JenKem Technology) at rt for 1 h. The amount of the PEG-MAL polymer added was 1/8 to 1/4 of the amount of remaining free thiols measured by the DTNB assay so that the undesired products can form tetramer to octamer. Pure Atx1-Tz, RBP-Tz, and MBP-Tz were obtained using size-exclusion chromatography (HiLoad 16/600 Superdex 75 pg column, GE Life Sciences). Atx1-Tz was eluted using 20 mM MES (pH 6.0) and 0.1 M NaCl buffer, and RBP-Tz and MBP-Tz were eluted using PBS (pH 7.4). The Bradford assay (protein assay dye reagent concentrate, BioRad) was used to determine the molar extinction coefficients of cross-linked proteins using standard curves generated by the corresponding non-cross-linked proteins. The extinction coefficients of Atx1-Tz, RBP-D67C/G134C-Tz, and MBP-Tz for concentration determination were 19,070 M^{-1} cm^{-1} at 283 nm, 19,290 M^{-1} cm^{-1} at 282 nm, and 75,870 M^{-1} cm^{-1} at 280 nm, respectively.

SDS-PAGE Analysis. Protein samples were mixed with 5× loading dye (10% SDS, 500 mM dithiothreitol, 50% glycerol, 250 mM Tris, pH 6.8, and 0.5% bromophenol blue dye) and boiled for at least 5 min before loading onto a 4−15% Mini-PROTEAN TGX precast protein gel (BioRad). For non-reducing SDS-PAGE, dithiothreitol was omitted from the loading dye. Precision Plus Protein (BioRad) was used as protein standards, and running buffer was prepared from 10× Tris/glycine/SDS buffer (BioRad). With the dye front near the bottom of the gel cassette, the gel was stained with Coomassie blue and destained in methanol/acetic acid/water.

DTNB Assay. DTNB (Thermo Scientific) was prepared as 4 mg/mL stock solution in 0.1 M sodium phosphate (pH 8.0) and 1 mM EDTA. Protein samples at 50−200 μM were mixed with 10 volumes of 0.1 M sodium phosphate (pH 8.0), 1 mM EDTA buffer, and 0.2 volumes of DTNB stock solution. Blank samples were prepared at the same time using protein storage buffers. After 15 min of incubation at room temperature, absorbance at 412 nm was measured using an Agilent Cary 3500 UV−vis spectrophotometer. Sulfhydryl concentration can be calculated using the molar extinction coefficient of TNB (14,150 M^{-1} cm^{-1} in 0.1 M sodium phosphate (pH 8.0), 1 mM EDTA) as [−SH] = Abs × 11.2/14150 M. The percentage of unreacted Cys was calculated as 0.5 × [−SH]/[protein].

Photolysis. Coast PX100 flashlight emitting 405 nm was used as the photolysis light source. Emission profile of the light source was obtained using a Varian Cary Eclipse fluorescence spectrophotometer (Figure S12). The photon flux density of the light source was determined using the potassium ferrioxalate chemical actinometer in a 1 cm quartz cuvette with a 2 mm × 2.5 mm window placed at 1 cm distance from the light source.[59] The photon flux density was (1.7 ± 0.1) × 10^{15} mm^{-2} s^{-1}. During photolysis, cross-linked and non-cross-linked protein samples at 10 μM in PBS (pH 7.4) were placed at a 1 cm distance from the light source. Kinetics measurements were carried out using an Agilent Cary 3500 UV−vis spectrophotometer.

^{129}Xe Hyper-CEST NMR. HP ^{129}Xe was generated using the spin-exchange optical pumping (SEOP) method[13] with a home-built ^{129}Xe polarizer based on the IGI.Xe.2000 commercial model by GE. A Shark 65 W tunable ultranarrow band diode laser (OptiGrate) set to 794.770 nm was used for optical pumping of Rb vapor. A gas mixture of 88% helium, 10% nitrogen, and 2% natural abundance xenon (Linde Group, NJ) was used as the hyperpolarizer input. The output ^{129}Xe hyperpolarization level was roughly 10%. For each data point in the hyper-CEST z-spectra, hp ^{129}Xe was bubbled into the NMR tube through capillaries for 20 s, followed by a 3 s delay to allow bubbles to collapse. A d-SNOB saturation pulse with a 690 Hz bandwidth was used. Pulse length, τ_{pulse} = 3.80 ms; field strength $B_{1,max}$ = 77 μT; number of pulses, n_{pulse} = 600; saturation time, T_{sat} = 2.28 s. NMR experiments were performed using a Bruker BioDRX 500 MHz NMR spectrometer and 10 mm PABBO probe at 300 K. A 90° hard pulse of this probe has a pulse length of 22 μs. Protein samples were in PBS (pH 7.4), with 0.1% (v/v) Pluronic L81 (Aldrich) added to mitigate foaming. For the time-dependent saturation transfer experiments, a 10 μM protein concentration was used. Pulse length, τ_{pulse} = 1.0496 ms; field strength, $B_{1,max}$ = 279 μT. The saturation frequency was set to ±60 ppm for MBP-Tz and ±65 ppm for MBP-BMOE. Both on-resonance and off-resonance data were fitted with first-order exponential decay curves. Saturation contrast (saturation transfer efficiency) was calculated as described before.[60] It represents the normalized difference between on- and off-resonance signals in saturation time-dependent hyper-CEST experiments, which is directly proportional to the MR image contrast. All results were averaged over at least three trials.

CD Spectroscopy. The CD spectra of the 10 μM protein sample were acquired in a 1 mm quartz cuvette using an Aviv Model 425 CD spectrometer. Data were recorded from 260 to 195 nm with a wavelength step of 1 nm and an averaging time of 15 s at 298 K.

Mass Spectrometry. The MS spectra were collected with a Bruker Ultraflex III TOF/TOF matrix-assisted laser desorption/ionization (MALDI) or a Bruker Microflex MALDI mass spectrometer. The matrix used was a saturated solution of sinapinic acid in 70% acetonitrile with 0.1% trifluoroacetic acid.

Dynamic Light Scattering (DLS). Samples of 10 μM protein were prepared in PBS (pH 7.4). The temperature was set to 298 K. Data were collected with a Zetasizer Nano Z system, and the volume (mass) distributions were averaged over at least three trials.

■ ASSOCIATED CONTENT

Supporting Information

The Supporting Information is available free of charge at https://pubs.acs.org/doi/10.1021/acsomega.4c00968.

Figures of size-exclusion chromatography, SDS-PAGE, MALDI-TOF MS, CD for all three native and cross-linked proteins, and also DLS and Xe-129 NMR characterization for native and cross-linked MBP (PDF)

■ AUTHOR INFORMATION

Corresponding Author

Ivan J. Dmochowski − *Department of Chemistry, University of Pennsylvania, Philadelphia, Pennsylvania 19104, United*

https://doi.org/10.1021/acsomega.4c00968
ACS Omega 2024, 9, 29331−29338

States; orcid.org/0000-0001-7162-1347;
Email: ivandmo@sas.upenn.edu

Authors

Zhuangyu Zhao − *Department of Chemistry, University of Pennsylvania, Philadelphia, Pennsylvania 19104, United States*

Nathan A. Rudman − *Department of Chemistry, University of Pennsylvania, Philadelphia, Pennsylvania 19104, United States*

Complete contact information is available at:
https://pubs.acs.org/10.1021/acsomega.4c00968

Notes

The authors declare no competing financial interest.

■ ACKNOWLEDGMENTS

This research was supported by NIH grant R35-GM-131907 to I.J.D. MD simulations in this work used the Extreme Science and Engineering Discovery Environment (XSEDE) supported by National Science Foundation grant number ACI-1548562, which now has transitioned to Advanced Cyberinfrastructure Coordination Ecosystem: Services & Support (ACCESS). Specifically, it used the Bridges-2 system, which is supported by NSF award number ACI-1928147, at the Pittsburgh Supercomputing Center (PSC). We thank Drs. Jun Gu and Chad W. Lawrence for assistance with NMR spectroscopy. We thank Dr. Charles W. Ross for mass spectrometry expertise.

■ REFERENCES

(1) Emiliani, V.; Entcheva, E.; Hedrich, R.; Hegemann, P.; Konrad, K. R.; Luscher, C.; Mahn, M.; Pan, Z. H.; Sims, R. R.; Vierock, J.; Yizhar, O. Optogenetics for Light Control of Biological Systems. *Nat. Rev. Methods Primers* **2022**, *2* (1), 55.

(2) Hoorens, M. W. H.; Szymanski, W. Reversible, Spatial and Temporal Control over Protein Activity Using Light. *Trends Biochem. Sci.* **2018**, *43* (8), 567−575.

(3) Ellis-Davies, G. C. R. Useful Caged Compounds for Cell Physiology. *Acc. Chem. Res.* **2020**, *53* (8), 1593−1604.

(4) Yang, L.; Dmochowski, I. J. Conditionally Activated ("Caged") Oligonucleotides. *Molecules* **2021**, *26* (5), 1481.

(5) Yamaguchi, S. Recent Advances in Protein Caging Tools for Protein Photoactivation. *Appl. Sci.* **2022**, *12* (8), 3750.

(6) Ritterson, R. S.; Kuchenbecker, K. M.; Michalik, M.; Kortemme, T. Design of a Photoswitchable Cadherin. *J. Am. Chem. Soc.* **2013**, *135* (34), 12516−12519.

(7) Shishido, H.; Yamada, M. D.; Kondo, K.; Maruta, S. Photocontrol of Calmodulin Interaction with Target Peptides using Azobenzene Derivative. *J. Biochem.* **2009**, *146* (4), 581−590.

(8) Hansen, K. C.; Rock, R. S.; Larsen, R. W.; Chan, S. I. A Method for Photoinitating Protein Folding in a Nondenaturing Environment. *J. Am. Chem. Soc.* **2000**, *122* (46), 11567−11568.

(9) Huang, J. J. T.; Larsen, R. W.; Chan, S. I. The Interplay of Turn Formation and Hydrophobic Interactions on the Early Kinetic Events in Protein Folding. *Chem. Commun.* **2012**, *48* (4), 487−497.

(10) Chen, R. P. Y.; Huang, J. J. T.; Chen, H. L.; Jan, H.; Velusamy, M.; Lee, C. T.; Fann, W. S.; Larsen, R. W.; Chan, S. I. Measuring the Refolding of beta-Sheets with Different Turn Sequences on a Nanosecond Time Scale. *Proc. Natl. Acad. Sci. U. S. A.* **2004**, *101* (19), 7305−7310.

(11) Rock, R. S.; Hansen, K. C.; Larsen, R. W.; Chan, S. I. Rapid Photochemical Triggering of Protein Unfolding in a Nondenaturing Environment. *Chem. Phys.* **2004**, *307* (2−3), 201−208.

(12) Tucker, M. J.; Courter, J. R.; Chen, J.; Atasoylu, O.; Smith, A. B., 3rd; Hochstrasser, R. M. Tetrazine Phototriggers: Probes for Peptide Dynamics. *Angew. Chem., Int. Ed. Engl.* **2010**, *49* (21), 3612−3616.

(13) Luo, J.; Samanta, S.; Convertino, M.; Dokholyan, N. V.; Deiters, A. Reversible and Tunable Photoswitching of Protein Function through Genetic Encoding of Azobenzene Amino Acids in Mammalian Cells. *ChemBioChem.* **2018**, *19* (20), 2178−2185.

(14) Schierling, B.; Noël, A. J.; Wende, W.; Hien, L. T.; Volkov, E.; Kubareva, E.; Oretskaya, T.; Kokkinidis, M.; Römpp, A.; Spengler, B.; Pingoud, A. Controlling the Enzymatic Activity of a Restriction Enzyme by Light. *Proc. Natl. Acad. Sci. U. S. A.* **2010**, *107* (4), 1361−1366.

(15) Goguen, B. N.; Hoffman, B. D.; Sellers, J. R.; Schwartz, M. A.; Imperiali, B. Light-Triggered Myosin Activation for Probing Dynamic Cellular Processes. *Angew. Chem., Int. Ed. Engl.* **2011**, *50* (25), 5667−5670.

(16) Banghart, M.; Borges, K.; Isacoff, E.; Trauner, D.; Kramer, R. H. Light-Activated Ion Channels for Remote Control of Neuronal Firing. *Nat. Neurosci.* **2004**, *7* (12), 1381−1386.

(17) Wu, Y. I.; Frey, D.; Lungu, O. I.; Jaehrig, A.; Schlichting, I.; Kuhlman, B.; Hahn, K. M. A Genetically Encoded Photoactivatable Rac Controls the Motility of Living Cells. *Nature* **2009**, *461* (7260), 104−108.

(18) Levskaya, A.; Weiner, O. D.; Lim, W. A.; Voigt, C. A. Spatiotemporal Control of Cell Signalling using a Light-Switchable Protein Interaction. *Nature* **2009**, *461* (7266), 997−1001.

(19) Seifert, S.; Brakmann, S. LOV Domains in the Design of Photoresponsive Enzymes. *ACS Chem. Biol.* **2018**, *13* (8), 1914−1920.

(20) Dagliyan, O.; Hahn, K. M. Controlling Protein Conformation with Light. *Curr. Opin. Struct. Biol.* **2019**, *57*, 17−22.

(21) Smart, A. D.; Pache, R. A.; Thomsen, N. D.; Kortemme, T.; Davis, G. W.; Wells, J. A. Engineering a Light-Activated Caspase-3 for Precise Ablation of Neurons *in vivo*. *Proc. Natl. Acad. Sci. U. S. A.* **2017**, *114* (39), E8174−E8183.

(22) Mayer, G.; Heckel, A. Biologically Active Molecules with a "Light Switch". *Angew. Chem., Int. Ed. Engl.* **2006**, *45* (30), 4900−4921.

(23) Nadendla, K.; Friedman, S. H. Light Control of Protein Solubility Through Isoelectric Point Modulation. *J. Am. Chem. Soc.* **2017**, *139* (49), 17861−17869.

(24) Baker, A. S.; Deiters, A. Optical Control of Protein Function through Unnatural Amino Acid Mutagenesis and Other Optogenetic Approaches. *ACS Chem. Biol.* **2014**, *9* (7), 1398−1407.

(25) Mart, R. J.; Allemann, R. K. Azobenzene Photocontrol of Peptides and Proteins. *Chem. Commun.* **2016**, *52* (83), 12262−12277.

(26) Szymanski, W.; Beierle, J. M.; Kistemaker, H. A.; Velema, W. A.; Feringa, B. L. Reversible Photocontrol of Biological Systems by the Incorporation of Molecular Photoswitches. *Chem. Rev.* **2013**, *113* (8), 6114−6178.

(27) Hoersch, D.; Roh, S. H.; Chiu, W.; Kortemme, T. Reprogramming an ATP-Driven Protein Machine into a Light-Gated Nanocage. *Nat. Nanotechnol.* **2013**, *8* (12), 928−932.

(28) Lee, H. M.; Larson, D. R.; Lawrence, D. S. Illuminating the Chemistry of Life: Design, Synthesis, and Applications of "Caged" and Related Photoresponsive Compounds. *ACS Chem. Biol.* **2009**, *4* (6), 409−427.

(29) Nadendla, K.; Sarode, B.; Friedman, S. H. Chemical Modification of Proteins with Photocleavable Groups. *Methods Enzymol.* **2019**, *624*, 113−128.

(30) Klan, P.; Solomek, T.; Bochet, C. G.; Blanc, A.; Givens, R.; Rubina, M.; Popik, V.; Kostikov, A.; Wirz, J. Photoremovable Protecting Groups in Chemistry and Biology: Reaction Mechanisms and Efficacy. *Chem. Rev.* **2013**, *113* (1), 119−191.

(31) Anttila, M. M.; Vickerman, B. M.; Wang, Q.; Lawrence, D. S.; Allbritton, N. L. Photoactivatable Reporter to Perform Multiplexed and Temporally Controlled Measurements of Kinase and Protease Activity in Single Cells. *Anal. Chem.* **2021**, *93* (49), 16664−16672.

(32) Ghosh, M.; Ichetovkin, I.; Song, X.; Condeelis, J. S.; Lawrence, D. S. A New Strategy for Caging Proteins Regulated by Kinases. *J. Am. Chem. Soc.* **2002**, *124* (11), 2440−2441.
(33) Nguyen, L. T.; Oien, N. P.; Allbritton, N. L.; Lawrence, D. S. Lipid Pools as Photolabile "Protecting Groups": Design of Light-Activatable Bioagents. *Angew. Chem., Int. Ed. Engl.* **2013**, *52* (38), 9936−9939.
(34) Weinstain, R.; Slanina, T.; Kand, D.; Klan, P. Visible-to-NIR-Light Activated Release: From Small Molecules to Nanomaterials. *Chem. Rev.* **2020**, *120* (24), 13135−13272.
(35) Goguen, B. N.; Imperiali, B. Chemical Tools for Studying Directed Cell Migration. *ACS Chem. Biol.* **2011**, *6* (11), 1164−1174.
(36) Clavier, G.; Audebert, P. *s*-Tetrazines as Building Blocks for New Functional Molecules and Molecular Materials. *Chem. Rev.* **2010**, *110* (6), 3299−3314.
(37) Loredo, A.; Tang, J.; Wang, L. S.; Wu, K. L.; Peng, Z.; Xiao, H. Tetrazine as a General Phototrigger to Turn on Fluorophores. *Chem. Sci.* **2020**, *11* (17), 4410−4415.
(38) Tucker, M. J.; Abdo, M.; Courter, J. R.; Chen, J.; Smith, A. B., 3rd; Hochstrasser, R. M. Di-Cysteine *S,S*-Tetrazine: A Potential Ultrafast Photochemical Trigger to Explore the Early Events of Peptide/Protein Folding. *J. Photochem. Photobiol. A Chem.* **2012**, *234*, 156−163.
(39) Abdo, M.; Brown, S. P.; Courter, J. R.; Tucker, M. J.; Hochstrasser, R. M.; Smith, A. B., 3rd. Design, Synthesis, and Photochemical Validation of Peptide Linchpins Containing the *S. S-Tetrazine Phototrigger. Org. Lett.* **2012**, *14* (13), 3518−3521.
(40) Brown, S. P.; Smith, A. B., 3rd. Peptide/Protein Stapling and Unstapling: Introduction of *s*-Tetrazine, Photochemical Release, and Regeneration of the Peptide/Protein. *J. Am. Chem. Soc.* **2015**, *137* (12), 4034−4037.
(41) Courter, J. R.; Abdo, M.; Brown, S. P.; Tucker, M. J.; Hochstrasser, R. M.; Smith, A. B., 3rd. The Design and Synthesis of Alanine-Rich alpha-Helical Peptides Constrained by an *S,S*-tetrazine Photochemical Trigger: a Fragment Union Approach. *J. Org. Chem.* **2014**, *79* (2), 759−768.
(42) Carboni, R. A.; Lindsey, R. V. Reactions of Tetrazines with Unsaturated Compounds. A New Synthesis of Pyridazines. *J. Am. Chem. Soc.* **1959**, *81*, 4342−4346.
(43) Bjorkman, A. J.; Binnie, R. A.; Zhang, H.; Cole, L. B.; Hermodson, M. A.; Mowbray, S. L. Probing Protein-Protein Interactions. The Ribose-Binding Protein in Bacterial Transport and Chemotaxis. *J. Biol. Chem.* **1994**, *269* (48), 30206−30211.
(44) Wang, C.; Liu, C.; Wei, Q.; Yang, L.; Yang, P.; Li, Y.; Cheng, Y. *S,S*-Tetrazine-Based Hydrogels with Visible Light Cleavable Properties for on-Demand Anticancer Drug Delivery. *Research* **2020**, *2020*, 6563091.
(45) Roose, B. W.; Zemerov, S. D.; Dmochowski, I. J. Nanomolar Small-Molecule Detection Using a Genetically Encoded ^{129}Xe NMR Contrast Agent. *Chem. Sci.* **2017**, *8* (11), 7631−7636.
(46) Zhao, Z.; Rudman, N. A.; He, J.; Dmochowski, I. J. Programming Xenon Diffusion in Maltose-Binding Protein. *Biophys. J.* **2022**, *121* (23), 4635−4643.
(47) Bjorkman, A. J.; Mowbray, S. L. Multiple Open Forms of Ribose-Binding Protein Trace the Path of its Conformational Change. *J. Mol. Biol.* **1998**, *279* (3), 651−664.
(48) Rubin, S. M.; Lee, S. Y.; Ruiz, E. J.; Pines, A.; Wemmer, D. E. Detection and Characterization of Xenon-Binding Sites in Proteins by ^{129}Xe NMR Spectroscopy. *J. Mol. Biol.* **2002**, *322* (2), 425−440.
(49) Reessing, F.; Stuart, M. C. A.; Samplonius, D. F.; Dierckx, R.; Feringa, B. L.; Helfrich, W.; Szymanski, W. A Light-Responsive Liposomal Agent for MRI Contrast Enhancement and Monitoring of Cargo Delivery. *Chem. Commun.* **2019**, *55* (72), 10784−10787.
(50) Phillips, J. C.; Braun, R.; Wang, W.; Gumbart, J.; Tajkhorshid, E.; Villa, E.; Chipot, C.; Skeel, R. D.; Kale, L.; Schulten, K. Scalable Molecular Dynamics with NAMD. *J. Comput. Chem.* **2005**, *26* (16), 1781−1802.
(51) Towns, J.; Cockerill, T.; Dahan, M.; Foster, I.; Gaither, K.; Grimshaw, A.; Hazlewood, V.; Lathrop, S.; Lifka, D.; Peterson, G. D.; et al. XSEDE: Accelerating Scientific Discovery. *Comput. Sci. Eng.* **2014**, *16* (5), 62−74.
(52) Nystrom, N. A.; Levine, M. J.; Roskies, R. Z.; Scott, J. R. Bridges: a Uniquely Flexible HPC Resource for New Communities and Data Analytics. In *Proceedings of the 2015 XSEDE Conference: Scientific Advancements Enabled by Enhanced Cyberinfrastructure*, Association for Computing Machinery: St. Louis, MO, 2015.
(53) Jorgensen, W. L.; Chandrasekhar, J.; Madura, J. D.; Impey, R. W.; Klein, M. L. Comparison of Simple Potential Functions for Simulating Liquid Water. *J. Chem. Phys.* **1983**, *79* (2), 926.
(54) Best, R. B.; Zhu, X.; Shim, J.; Lopes, P. E.; Mittal, J.; Feig, M.; Mackerell, A. D., Jr. Optimization of the Additive CHARMM All-Atom Protein Force Field Targeting Improved Sampling of the Backbone phi, psi and Side-Chain chi(1) and chi(2) Dihedral Angles. *J. Chem. Theory. Comput.* **2012**, *8* (9), 3257−3273.
(55) Verlet, L.; Weis, J.-J. Perturbation Theory for the Thermodynamic Properties of Simple Liquids. *Mol. Phys.* **1972**, *24* (5), 1013−1024.
(56) Ryckaert, J.-P.; Ciccotti, G.; Berendsen, H. J. C. Numerical Integration of the Cartesian Equations of Motion of a System with Constraints: Molecular Dynamics of n-Alkanes. *J. Comput. Phys.* **1977**, *23* (3), 327−341.
(57) Humphrey, W.; Dalke, A.; Schulten, K. VMD: Visual Molecular Dynamics. *J. Mol. Graph.* **1996**, *14* (1), 33−38.
(58) Gasteiger, E.; Hoogland, C.; Gattiker, A.; Duvaud, S.; Wilkins, M. R.; Appel, R. D.; Bairoch, A. Protein Identification and Analysis Tools on the ExPASy Server. In *The Proteomics Protocols Handbook*, Walker, J. M. Ed.; Humana Press, 2005; pp 571−607.
(59) Hatchard, C. G.; Parker, C. A. A New Sensitive Chemical Actinometer - II. Potassium Ferrioxalate as a Standard Chemical Actinometer. *Proc. R. Soc. London, Ser. A* **1956**, *235* (1203), 518−536.
(60) Wang, Y.; Roose, B. W.; Palovcak, E. J.; Carnevale, V.; Dmochowski, I. J. A Genetically Encoded β-Lactamase Reporter for Ultrasensitive ^{129}Xe NMR in Mammalian Cells. *Angew. Chem., Int. Ed. Engl.* **2016**, *55* (31), 8984−8987.

https://doi.org/10.1021/acsomega.4c00968
ACS Omega 2024, 9, 29331−29338